Available online at www.sciencedirect.com
SCIENCE DIRECT®
International Journal of Heat and Mass Transfer 47 (2004) 5391–5406
International Journal of HEAT and MASS TRANSFER
www.elsevier.com/locate/ijhmt

Spray cooling in a closed system with different fractions of non-condensibles in the environment

Shanjuan Jiang, Vijay K. Dhir *

Mechanical and Aerospace Engineering Department, Henry Samueli School of Engineering and Applied Science, University of California, Los Angeles, 420 Westwood Plaza, Los Angeles, CA 90095, USA

Received 6 January 2004; received in revised form 15 July 2004
Available online 16 September 2004

Abstract

Spraying liquid on a hot surface is an effective method for dissipating high heat fluxes from integrated circuit chips. In this study, HAGO nozzle was used to create the spray and a closed system with water as a test liquid was used. The effect of presence of non-condensibles in the closed system on the heat transfer coefficient in both single phase and boiling modes were investigated. Maintaining an air partial pressure of 3.1 kPa, while varying the vapor partial pressure from 7.3 kPa to 97.9 kPa, the total system pressure was varied from 10.4 kPa to 101 kPa. Experiments were also conducted by keeping the system pressure constant at 101 kPa and varying the air partial pressure inside the chamber from 2.75 kPa to 93.7 kPa. In each case, liquid temperature corresponded to the saturation temperature corresponding to partial pressure of vapor and this was also approximately the ambient temperature of vapor and air mixture in the chamber. It was found that in the single phase regime, overall heat transfer coefficient for lower concentration of non-condensibles in the system is much higher than that for the case with more non-condensibles. In boiling, heat transfer coefficient depends on the total system pressure in the system. For the same system pressure, data for different partial pressures of air overlap. For a water mass flux of 17.5 ml/min/cm^2 at room temperature, critical heat flux as high as 230 W/cm^2 was obtained at a surface temperature of 127 °C.

Keywords: Non-condensibles; Spray cooling; Closed system

1. Introduction

It is known that spraying of liquid on a hot surface is an effective means of dissipating high heat fluxes from the surface. A number of investigations have been performed for spray cooling under different conditions. However, a review of the literature reveals that very limited data are available for spray cooling in a closed system. For use of spray cooling in electronic packaging, the system will have to be closed.

Choi and Yao [1,2] conducted experiments on mist flows and sprays in the high surface temperature regime when heat transfer occurs by film boiling. Normally impacting sprays and vertical impacting sprays were employed by Choi and Yao. They used a piezoelectric generator to break the water jet into uniform size droplets impinging on a copper block with a chrome plated surface. An air supply was used to make the liquid droplets

* Corresponding author. Tel.: +1 310 825 8507/9617; fax: +1 310 206 4830.
E-mail address: vdhir@seas.ucla.edu (V.K. Dhir).

0017-9310/$ - see front matter © 2004 Elsevier Ltd. All rights reserved.
doi:10.1016/j.ijheatmasstransfer.2004.07.013

Nomenclature

A	heating area (m^2)
c_1, c_2	constants
c_p	specific heat (J/kg K)
D	heater diameter (m)
h	heat transfer coefficient ($W/m^2 K$)
h_{fg}	heat of vaporization (J/kg)
k	thermal conductivity (W/mK)
Nu	Nusselt number
p	pressure (Pa)
Pr	Prandtl number
$Q_{pumping}$	pumping power (W)
$Q_{removed}$	power removed from surface (W)
Q_{total}	total heat input (W)
q	heat flux (W/cm^2)
$\dot{m}_l$	liquid mass flux ($kg/s/mm^2$)
Re	Reynolds number
T	temperature (°C)
ΔT	temperature difference (°C)
$\dot{V}$	volume flow rate ($ml/s/mm^2$)
Δx	distance (m)

Greek symbols

δ	liquid film thickness (μm)
ε	heat transfer effectiveness
μ	dynamic viscosity (kg/m/s)
v	kinematic viscosity (m^2/s)
ρ	density (kg/m^3)
σ	surface tension (N/m)

Subscripts

air	air pressure
e	ambient
i	interface
l	liquid
g	gas
sat	saturation
T	temperature
total	total pressure
v	vapor phase
w	wall

disperse properly and to accelerate the droplets. Water was at room temperature (24 °C) and the droplet size ranged from 0.407 to 0.530 mm. The effects of liquid mass flux, impinging velocity, droplet size, and air convection on the total rate of heat transfer were studied. At low liquid mass fluxes (less than 0.0376 g/cm^2 s), the critical heat flux (CHF) was observed to occur at a wall temperature (T_w) of 135 °C. At higher wall temperatures, the heat flux decreased with a minimum occurring at 260 °C. Beyond this temperature, the heat flux was almost constant and independent of surface temperature. At liquid mass fluxes higher than 0.0376 g/cm^2 s, the wall temperature at CHF increased to 145–155 °C. The minimum heat flux occurred at 260 °C just as in case for low liquid mass fluxes. The critical heat flux increased with increase in liquid mass flux. Droplet velocity was varied through axial acceleration of the droplets by the modified air supply system. It was observed that the effect of velocity in film boiling regime was insignificant. As a result, the details of impact dynamic became less significant. The effect of droplet size was studied while varying the diameter from 0.41 to 0.49 mm. No significant effect was observed on the rate of heat transfer. The heat transfer effectiveness (ε) was defined as the ratio of the actual heat transfer due to the effect of impinging droplets to the overall energy that is required for complete evaporation of the liquid droplets

$$\varepsilon = \frac{q}{\dot{m}_l (h_{fg} + c_{pl}\Delta T_w)} \tag{1}$$

where $\dot{m}_l$ (g/cm^2/s) is the liquid mass flux, h_{fg} is the latent heat of evaporation, c_{pl} is the specific heat of liquid, ΔT_w is the wall super heat and q (W/cm^2) is the wall heat flux. The effectiveness was found to decrease with mass flux. Droplet size and velocity had little influence. They correlated the film boiling heat flux (surface temperature beyond 260 °C) with liquid mass flux in the form

$$q = 170(\dot{m}_l)^{0.76} \tag{2}$$

The range of liquid mass flux was between 0.0091 and 0.21 g/cm^2/s.

In the regime of intermediate surface temperature when nucleate boiling occurs, spray cooling was studied by Kopchikov et al. [3]. Droplets were seen to partially contact the surface, either through continuous bubble nucleation, or through intermittent liquid contacts.

In their experiments, ethanol, carbon tetrachloride, benzene and distilled water were used for spray cooling of a brass surface. Closed system saturation pressures ranged from 8.08 kPa to 101 kPa. The size of spray nozzle ranged from 0.02 to 0.2 mm. The liquid flow rates were not specified in their paper. The surface was rough enough so that there were a considerable number of nucleation sites on the heater surface. The investigation showed that the peak heat flux was five times higher than that for pool boiling. It was also shown that the slope of heat transfer coefficient, h, vs. heat flux, q, was less steep for boiling in a liquid film than it was under pool boiling. For spray cooling using water as the test liquid, CHF occurred at a temperature difference

($T_w - T_l$) of 120 °C, which for pool boiling of saturated water at one atmosphere pressure corresponds to the minimum heat flux (Leidenfrost point). Upon reaching this temperature, continuous liquid film could not be maintained on the heated surface. However, the supply liquid temperature did not have a significant influence on the magnitude of the CHF. The boiling heat transfer coefficient for different liquids was studied at a number of pressures. It was found that the CHF decreased with decrease in system pressure. Assuming that the liquid is viscous, the thermal layer thickness of the layer adjacent to the bubble growth region, δ_T, is obtained as,

$$\delta_T = c_1 \frac{\sigma T_{sat(v)}}{\rho_v h_{fg}(T_w - T_l)} \tag{3}$$

where c_1 is a constant and $T_{sat(v)}$ is the vapor saturation temperature. As $h = q_w/(T_w - T_l)$, the heat transfer coefficient corresponding to a linear temperature profile was found to be,

$$h = c_2 \left(\frac{k\rho_v h_{fg}}{\sigma T_{sat(v)}} q_w \right)^{1/2} \tag{4}$$

where q_w is the heat flux. Empirical constant c_2 was found to be about 0.1. The correlation agreed with the experimental data for all liquids and pressures. They also investigated the burnout phenomena. But in their paper, they did not specify what kind of closed system was used to operate the spray and what was the fraction of non-condensibles in the system. They found that conditions for the onset of burnout were associated with the limiting temperature to which liquid could be superheated. They stated that when boiling occurs in a liquid film, burnout is a thermodynamic process and there are hydrodynamic restrictions on the removal of the vapor phase and supply of the liquid phase. Burnout occurs at the moment when the surface temperature reaches the limiting value corresponding to maximum possible superheat for the liquid phase.

More recently, Pais et al. [4] and Sehmbey et al. [5] investigated the effects of surface thermal properties and contact angle on heat transfer in spray cooling. In their experiments, a gas-atomizing nozzle was used for spraying. According to their work, this type of nozzle has two advantages. First, the air jet forms a stagnation point flow field. The droplets do not follow the air streamlines close to the surface due to their high inertia, but impinge on the surface to form flat disks. The film thickness is much smaller than the droplet diameter. Simultaneously, the flow field due to air spreads the disk further through shear force to form a thinner film. Second, the air flow field helps sweep away the emanating vapor. Consequently, the bulk vapor pressure near the free liquid surface is reduced and the rate of evaporation is enhanced. They used three kinds of surfaces: these were oxygen-free copper surface polished with 14-μm grit paper, electroplated nickel surface on copper block and electroplated gold surface on nickel. The sprayed liquid was deionized water. The droplet sizes ranged from 7 to 25 μm. They obtained heat flux data as a function of wall temperature for different coolant flow rates, air flow rates, and degrees of liquid subcooling. A maximum heat flux of 650 W/cm^2 in a 9×9 mm^2 area, for an air flow rate of 2 ml/s/mm^2 and water flow rate of 0.014 ml/s/mm^2, was achieved. They observed that with increasing contact angle the heat transfer rate increased due to enhanced boiling.

At surface temperatures which are lower than the liquid saturation temperature, boiling is absent. The mode of heat transfer is mainly convection with some evaporation.

In this regime, Bonacina et al. [6] conducted a study on multi-drop evaporation. In their experiments, a dilute spray was used so that no coalescence of liquid droplets on the heated surface took place. The average droplet size was ~400 μm and the impinging velocity was 1–2 m/s. The fraction of the heat transfer area covered by droplets was obtained through photographic observation. The measured heat flux was found to be proportional to the fraction of the solid surface wetted by the spray. Heat transfer coefficients up to 15 W/cm^2 K and heat flux up to 220 W/cm^2 were obtained. Based on assumptions of droplet evaporation via heat conduction through the liquid patches on the heater surface, and Rosin–Rammler distribution of droplet size in the spray, heat flux for multi-droplets impinging on the surface was calculated as a function of droplet size and the fraction of heat transfer area covered by droplets. The measured heat flux data were shown to match well with the predictions.

Grissom and Wierum [7] conducted experiments in a closed system and found that the lowest surface temperature at which all of the impinging spray (non-flooding) droplets vaporize is a linear function of the impinging spray mass flux. In their experiments, distilled water at 25 °C was sprayed on to a heated aluminum surface. The mass-weighted average droplet diameter was 155 μm at atmospheric pressure. Spray cooling measurements were made by applying power to the heater surface of an aluminum cylinder and adjusting the spray so that the surface would be just covered with a thin liquid film. Data at pressures of 101 kPa and low pressure of 0.9 kPa ($T_{sat}(P_{total}) = 6$ °C) were obtained. They found that at reduced pressures, droplet evaporation rates decreased significantly such that an optimum operating pressure existed for each desired surface heat flux. With boiling, the surface heat flux showed a linear relationship with $T_w - T_l$ and appeared to be independent of the liquid mass flux. However, in their experiments, the determination of liquid mass flux required to just cover the surface with a liquid film was by visual observation. The uncertainty of which was reflected in the

scatter in the data. At low pressures, they did not specify the extent of non-condensibles in the closed system.

Estes and Mudawar [8,9] performed experiments in a closed system. In their setup, the chamber was closed, and a condenser was placed inside the test chamber to maintain a pressure of 1 atm. Based on data obtained over a broad range of water flow rates and for different spray types, including full cone, hollow cone and flat sprays, they developed a correlation for critical heat flux with water as the test liquid as,

$$\frac{q_{\mathrm{CHF}}}{\rho_{\mathrm{v}} h_{fg} \dot{V}} = 2.3 \left(\frac{\sigma}{\rho_{\mathrm{l}} \dot{V}^2 d_{\mathrm{orifice}}} \right)^{0.35} \left(\frac{\rho_{\mathrm{l}}}{\rho_{\mathrm{v}}} \right)^{0.3} \times \left(1 + 0.0019 \frac{\rho_{\mathrm{l}} c_{p,\mathrm{l}} \Delta T_{\mathrm{sub}}}{\rho_{\mathrm{v}} h_{fg}} \right) \quad (5)$$

where $\dot{V}$ is the volumetric flux of liquid in ml/s/mm^2 and ΔT_{sub} is the liquid subcooling, $T_{\mathrm{sat}} - T_{\mathrm{l}}$.

The highest CHF obtained was 600 W/cm^2 for liquid flux of 0.005 ml/s/mm^2 and orifice size of 0.491 mm. But in their paper, it was not stated how well the system was isolated from the outer environment. In their experiments, they did not quantify the extent of the non-condensibles in the closed system.

From the literature review, it can be seen that most of the researchers have concentrated on spray cooling in open systems. Very few studies that have been conducted with a closed system have given any quantitative values for the non-condensibles present in the closed system. The objective of this work is to study the heat transfer behavior of sprays in a closed system at different system pressures and with varying fractions of non-condensibles in the system.

2. Experiments

2.1. Apparatus

The experimental apparatus is shown in Fig. 1. The test loop consists of a test chamber, a copper block the top surface of which served as the test surface, liquid reservoir, liquid pump, and a heat exchanger. The loop was tested for leakage under vacuum before each experiment. The closed system test chamber consists of a top plate and four side plates made of stainless steel plates that are welded together at the edge and form a square enclosure. The side plates are also welded at the base to a stainless steel flange. A bottom stainless steel plate is bolted to the flange by screws. An O-ring is placed between the steel flange and the bottom steel plate that gives a good vacuum seal. Upper cylindrical portion of the copper block whose top surface acts as test surface is surrounded by a Teflon sleeve. This Teflon sleeve is bolted to the bottom plate. Between the bottom flange and the Teflon support an O-ring is placed for vacuum seal. A groove for an O-ring is machined inside of the Teflon support so that it seals the gap between the copper block and the Teflon support. The copper block consists of a bottom cylindrical portion, which has a diameter of 60 mm and is 35 mm in height and a long cylindrical portion on top with a diameter of 20 mm and 40 mm in height. The long cylindrical portion was designed so as to obtain a linear temperature profile. Four thermocouples holes 0.76 mm in diameter drilled along the center line of the long cylindrical portion at a distance of 1 mm, 11 mm, 21 mm and 31 mm from the test surface. Chromel–alumel thermocouples with a

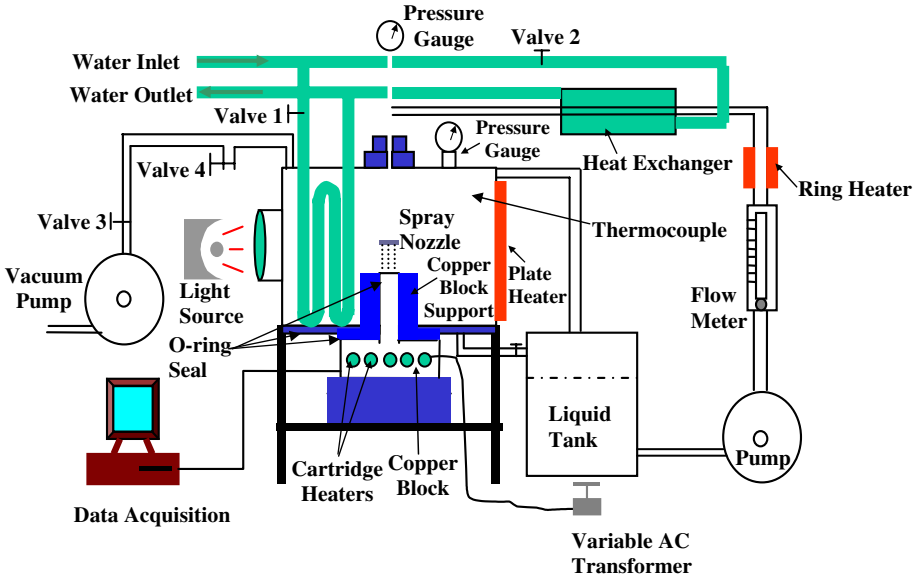

Fig. 1. Experimental apparatus for close system setup.

sheath diameter of 0.76 mm were brazed into the copper block. The copper block is heated from the bottom with five cartridge heaters. Each cartridge heater has a maximum power rating of 750 W. The heaters are connected to a 240 VAC variac that regulates the input power. Prior to each experiment, the copper surface was polished with 600 grit sandpaper and was oxidized. Oxidizing improves the wettability of the surface. The contact angle was found to be about 45° after the surface was oxidized.

Plate heaters are attached to the outer wall to control the rate of condensation or heat loss to the ambient. This in turn allows a better control on the system pressure. The power to the plate heaters is controlled with a feed back controller. A thermocouple placed inside the chamber gives the temperature input to the controller. The controller then compares the measured temperature with the desired preset value and based on the temperature difference controls the power to plate heaters. The temperature in the chamber is also set to the saturation temperature according to the desired vapor partial pressure in the chamber. The controller turns the heaters on when the temperature inside the chamber is lower than the desired value and vice versa. The system pressure inside the chamber is monitored with an absolute pressure gauge. A viewport window is welded at one side of the chamber wall for visual observation of the spray impinging on the test surface.

When the system pressure is higher than the desired value, the chilled water supply (12 °C) is opened manually and chilled water flows inside the copper coil placed inside the chamber. This cooling coil is used to condense excess vapor present inside the chamber. The rate of condensation can be adjusted by controlling the chilled water flow rate.

Deionized water is boiled for 1 h to be degassed before it is stored in a stainless steel tank. Water temperature is held constant at the desired value by adjusting the heating (through ring heater) and cooling (through heat exchanger). Water is sprayed from the nozzle normal to the heating surface and the distance between nozzle and heating surface is kept at 13 mm. The storage tank is connected to the test chamber to equalize the pressures in the chamber and in the tank. The vapor is condensed inside the chamber, drained from the bottom pipe to the tank and then recirculated by the pump to the nozzle again.

The nozzle used in the study is a commercially available humidifying nozzle by HAGO Nozzle Company. The specific type of the nozzle used in this study is DFN B100. The DFN-B100 nozzle was originally designed for use with home power spray humidifiers and is designed for low flow rates from 0.315 ml/min to 1.05 ml/min. It employs the two sintered bronze filters, which give more surface filtration. The nozzle produces the finest possible atomization with direct water pressure operation. The minimum operating pressure is 274.8 kPa gage pressure but increasingly finer droplets result from higher operating pressures. Different flow rates were tested and calibrated at a gage pressure of 274.8 kPa, with water as the test liquid. Each nozzle was individually spray tested for flow rate, spray angle and spray quality. Standard spray angle is 70° at 274.8 kPa gage pressure and will not change when operated at higher pressures (<3400 kPa). The Sauter mean diameter of droplets for the DFN-B100 nozzle at minimum operating pressure 274.8 kPa gage pressure is 44 μm according to the manufacturer.

2.2. Experimental procedure and data reduction

1. The test chamber was tested for vacuum leak before each experiment. The test chamber was evacuated down to around 2728 Pa. The chamber sealing was considered to be satisfactory if the increase in pressure due to leakage of air was less than 20 Pa in 1 h.
2. After the vacuum test, valve 4 (Fig. 1) was opened to the ambient and outside air was allowed to enter the chamber until the desired air (non-condensibles) pressure was achieved. Thereafter valve 4 was closed.
3. The chamber temperature was then set to the temperature corresponding to desired vapor partial pressure in the chamber. The test liquid (water) temperature was set to saturation temperature corresponding to vapor partial pressure. The power to the cartridge heaters in the copper block was then turned on. The liquid was then pumped from the reservoir to the nozzle and sprayed onto the heated surface. Part of water evaporated as it flowed over the heater surface. Evaporation of the liquid caused the chamber pressure to build up.
4. When the total pressure inside the chamber exceeded the desired value, valve 1 was opened and chilled water passed through cooling coil. As a result, the vapor inside the chamber condensed on the cooling coil leading to a drop in pressure inside the chamber. By adjusting the chilled water flow rate through the cooling coil, total system pressure in the chamber could be maintained at a desired value.

2.3. Uncertainty analysis

The heat flux was obtained from the temperature gradient measured along the centerline of the upper portion of the copper block using a linear fit of the output of the four thermocouples, i.e.,

$$q = -k\frac{\Delta T}{\Delta x} \tag{6}$$

The uncertainty was calculated to be about ±4.3% at a heat flux of 1 W/cm^2, and ±0.2% when the heat flux was 130 W/cm^2. The higher the heat flux, the lower is the uncertainty. The surface temperature was calculated by extrapolating the measured interior temperatures to the surface. The overall uncertainty in the surface temperature at 80 °C was found to be about ±0.8 °C. Heat transfer coefficient, h, is calculated as heat flux divided by temperature difference from the heater surface to the ambient,

$$h = q/(T_w - T_e) \tag{7}$$

At a heat flux of about 130 W/cm^2, and a surface temperature of about 80 °C, the uncertainty in heat transfer coefficient was calculated to be less than 0.05 W/cm^2 K. Maximum uncertainty in the measurement of chamber partial pressure is ±3%. Heat loss from the copper block was always found to be less than 10%. Details for uncertainty calculation are given by Jiang [10].

3. Results and discussions

In the closed system, vapor could not escape the chamber nor could outside air get into the chamber. The cooling coil condensed the vapor which kept the system pressure constant. Experimental data were first obtained for the HAGO nozzle using the open system setup, when the spray was operated in the ambient air. In order to compare the spray cooling in a closed system with an open system, under the same conditions, an experiment was conducted in the closed system without evacuating the chamber while it contained air at atmospheric pressure.

When initially the chamber contained air at 1 atm pressure (~101 kPa), the chamber pressure could be kept constant at about 101 kPa by using the condenser, when surface temperature was less than 100 °C. Above 100 °C, evaporation became very strong, and the condenser was not able to condense all the vapor produced, as a result, the chamber pressure started to increase slowly. At CHF, the chamber pressure was around 113 kPa. Both the open system and closed system data, when the chamber contained mostly air were compared and the two sets of data were found to overlap. It demonstrated that closed system could be used to simulate open system conditions when the closed system is filled with air and system pressure is held constant.

Using the closed system, experiments were conducted for total system pressures of 101 kPa, 72.5 kPa and 56 kPa and by varying the vapor partial pressure from 97.9 kPa to 2.32 kPa. Experiments were also performed at different total system pressures varying from 10.4 kPa to 101 kPa, while keeping the air partial pressure constant at 3.1 kPa. The experimental results are discussed in the following sections.

3.1. Heat transfer for fixed system pressures

In keeping the same system total pressure (56 kPa, 72.5 kPa and 101 kPa) while varying the vapor pressure inside the chamber from 2.32 kPa to 97.9 kPa, as a result, the corresponding ratio of partial pressure of air, $\frac{p_{air}}{p_{total}}$, in the closed system was varied from 3% to 98% for 101 kPa system pressure, from 4.27% to 90% for 72.5 kPa and from 5.5% to 87% for 56 kPa. The water spray temperature was varied from 23 °C to 100 °C which corresponds to the saturation temperatures for partial pressures of 2.32 kPa to 97.9 kPa.

Data for a flow rate of about 0.003 ml/s/mm^2 at 101 kPa total pressure are plotted in Fig. 2. The last data point is the dry out point. It can be seen from Fig. 2 that in the single phase regime, heat transfer coefficient is constant and independent of $T_w - T_l$. It is found that the data points for each $\frac{p_{air}}{p_{total}}$ value fall in a straight line. A linear best fit is also drawn on the graph for each $\frac{p_{air}}{p_{total}}$ value. When boiling starts, the slope of the heat transfer curve begins to deviate from the single phase regime and continues to increase until fully developed nucleate boiling occurs. Thereafter it remains almost constant until CHF is reached. It can be seen from the curves that for $\frac{p_{air}}{p_{total}}$ of 98%, the change in the slope is more discernible than for $\frac{p_{air}}{p_{total}}$ of 3%. A dotted line is drawn on the graph to distinguish the observed linear single phase regime and the possible partial nucleate boiling regime.

Experimental runs were also made for a flow rate about 0.003 ml/s/mm^2 at total pressures of 56 kPa and 72.5 kPa. The data for both was very similar to that in Fig. 2.

It was found that, for the same system pressure, the overall heat transfer coefficient for $\frac{p_{air}}{p_{total}} \sim 3\%$ is almost five times higher than that for $\frac{p_{air}}{p_{total}} \sim 98\%$. It was also noted that for the same vapor partial pressure, but at different total system pressure, smaller values of $\frac{p_{air}}{p_{total}}$ give higher overall heat transfer coefficient. These data are listed by Jiang [10].

The present closed system experimental data are compared with Mudawar et al.'s [9] data at a system pressure of 101 kPa. As shown in Fig. 3, for $(T_w - T_l) = 10$ °C, when the partial pressure of air, p_{air}, is 3.1 kPa, the heat flux is almost three times that of Mudawar et al.'s obtained in the closed system, even though the water flow rate in their work was two times higher than that in the current study. When p_{air} is 98.7 kPa, the heat flux is about 50% less than that in Mudawar et al.'s experiments in the closed system. In their experiments, the non-condensibles in the close system were not specified. It is argued here that higher heat transfer rate for low partial pressures of air is the result of strong evaporation from the liquid–vapor/gas interface into the ambient.

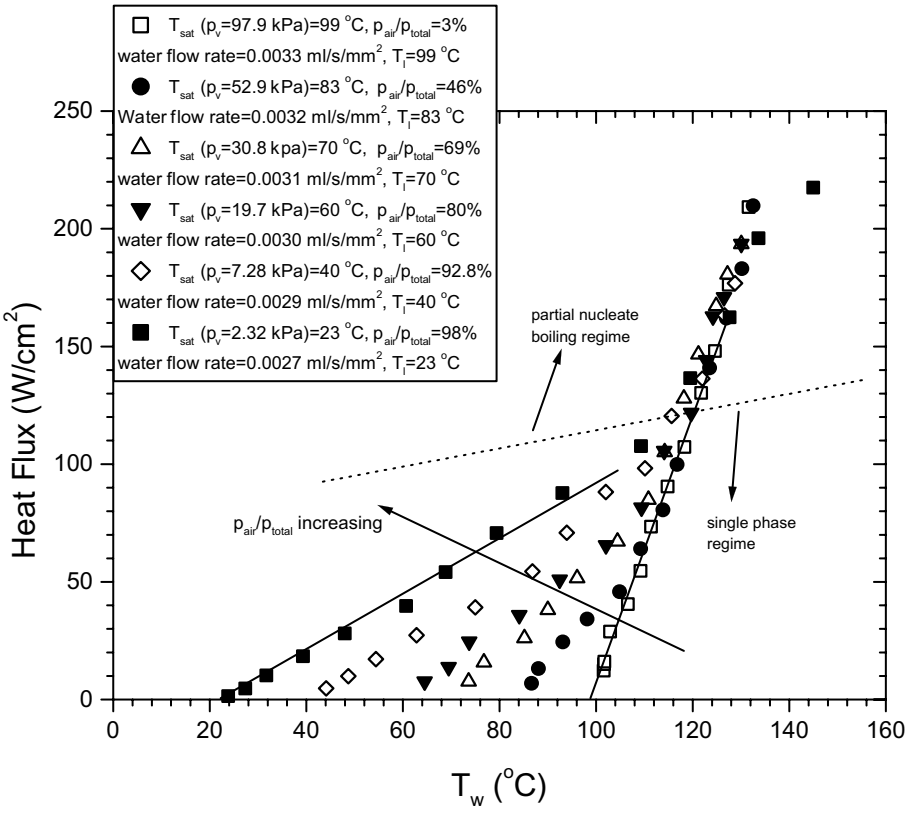

Fig. 2. Heat flux vs. surface temperature for (a) flow rate about 0.0027 ml/s/mm^2 at system pressure of 101 kPa.

In single phase regime, the overall heat transfer coefficient is defined as:

$$h = \frac{q}{T_w - T_l} \cong \frac{q}{T_w - T_e} \cong \frac{q}{T_w - T_{sat(v)}} \tag{8}$$

where, T_l, is the spray temperature as well as the saturation temperature, $T_{sat(v)}$ corresponding to the partial pressure of vapor in the chamber for a closed system. This is also the environment temperature, T_e. The linear behavior of data in the single phase regime implies that overall heat transfer coefficient is constant along the heat transfer curve.

We can correlate the Nusselt number, *Nu*, as a function of Reynolds number, *Re*, and Prandtl number, *Pr*. Nusselt number, *Nu*, and Reynolds number, *Re*, are defined based on the heater diameter as,

$$Nu = \frac{hD}{k} \tag{9}$$

$$Re = \frac{(\dot{V}/A)D}{v} \tag{10}$$

where A is the heater area, D is the diameter of the heater surface, k is the thermal conductivity of the liquid, $\dot{V}$ is the liquid volume flow rate and v is the liquid kinematic viscosity. Diameter of droplet is probably a better parameter to define Reynolds and Nusselt numbers but there can be a significant uncertainty associated with it. Fluid properties are evaluated at mean value of wall temperature and spray temperature.

A correlation for Nusselt number, Nu_0, that is free of evaporation can only be derived in terms of *Re* and *Pr* by using those experimental data for which little or no evaporation is believed to occur. It is believed that when ratio of partial pressure of air in the chamber, $\frac{p_{air}}{p_{total}}$, is very close to 100%, and heater surface temperature is low, very small amount of heat goes into evaporation. Using experimental data ($\frac{p_{air}}{p_{total}}$ varying from 90% to 98%) for low surface temperatures, a correlation for Nu_0 as a function of *Re* and *Pr* is obtained as,

$$Nu_0 = 9.75 Re^{0.7} Pr^{1/3} \tag{11}$$

Eq. (11) correlates data within ±10%. The Reynolds number ranges from 1000 to 2000 and Prandtl number ranges from 1.76 to 6.7 in this correlation.

When evaporation at the interface becomes significant, the overall heat transfer coefficient depends not only on thermophysical properties (viscosity, thermal conductivity, density and specific heat) but also on the

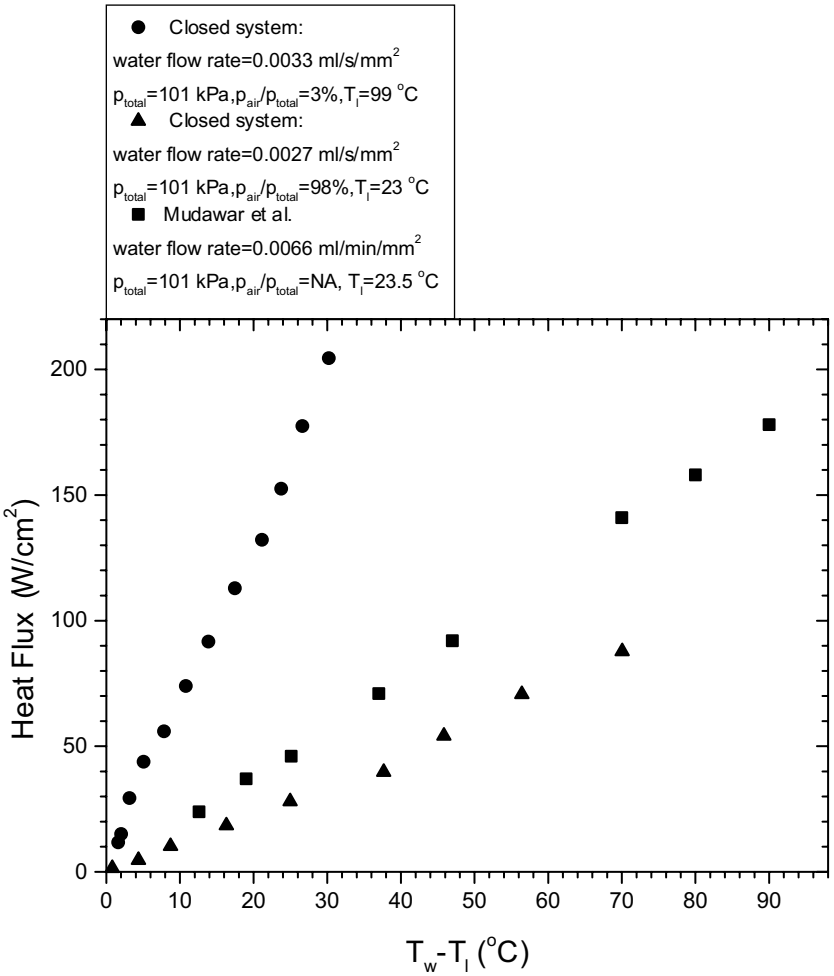

Fig. 3. Comparison between results from current study with those of Mudawar et al. [9].

evaporation rate. Since Nu_0 as a function of Reynolds number and Prandtl number includes the effect of thermophysical properties which are evaluated at the mean film temperature, the effect of partial pressure of air for the case in which evaporation is not zero, can be obtained by dividing the observed Nu with Nu_0. In Fig. 4, $\frac{Nu}{Nu_0}$ is plotted as a function of $\frac{p_{air}}{p_{total}}$ for three total pressures and two flow rates.

It is seen that $\frac{Nu}{Nu_0}$ increases as $\frac{p_{air}}{p_{total}}$ decreases. Data for different system pressures fall on the same curve. For the range of pressures studied, there is no obvious effect of system pressure on the overall heat transfer coefficient.

The increase in Nusselt number is a result of correction to the temperature profile in the liquid film that occurs due to evaporation at the interface. The effect of reduced time averaged film thickness is expected to be of second order as the rate of liquid lost due to evaporation is much smaller than the overall liquid flow rate.

The normalized Nusselt number, $\frac{Nu}{Nu_0}$, for flow rate of about 0.0029 ml/s/mm^2 and for $\frac{p_{air}}{p_{total}} \sim 3\%$ is four times higher than that for $\frac{p_{air}}{p_{total}} \sim 98\%$. This large difference between the two cases can only be attributed to evaporation that occurs on the interface as partial pressure of air in the system reduces. For a flow rate of about 0.0045 ml/s/mm^2, the increase of normalized Nusselt number is less (about three times). This is reflective of the fact that more energy is utilized for sensible heating at higher flow rates than at lower flow rate. As a result, the effect of evaporation is not as strong. The temperature profiles in the liquid film with and without evaporation are qualitatively shown in Fig. 5.

With evaporation, a significant increase in the temperature gradient at the wall occurs in comparison to the case without evaporation because of the significant amount of heat that is lost at the interface to support evaporation. Because only a small fraction of liquid is

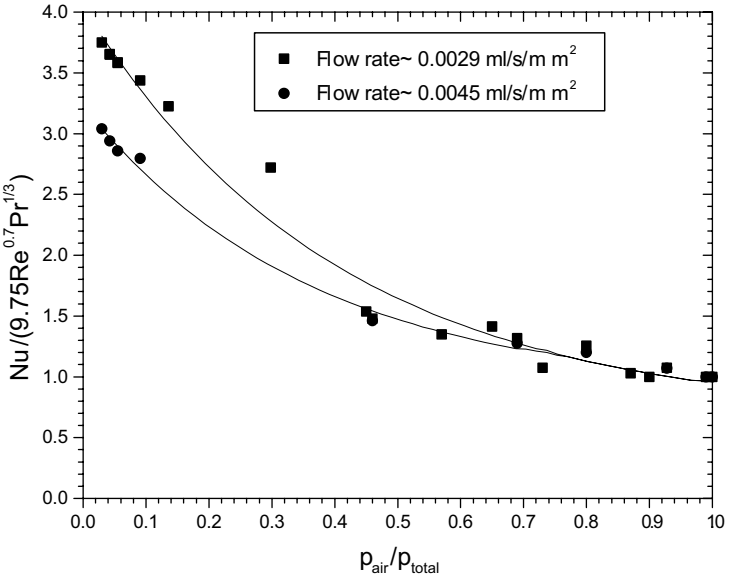

Fig. 4. Normalized Nusselt number as a function for $\frac{p_{air}}{p_{total}}$.

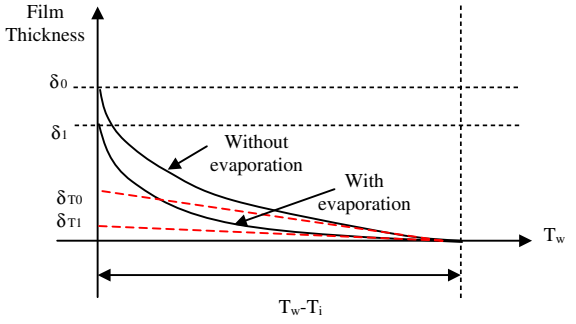

Fig. 5. Qualitative quasi-static temperature profiles in the liquid film for $\frac{p_{air}}{p_{total}} \sim 3\%$ and $\frac{p_{air}}{p_{total}} \sim 98\%$ at the same $T_w - T_i$.

evaporated, the effect of reduced film thickness with evaporation is expected to be small. As wall temperature (or heat flux) is increased for any partial pressure of air, it is not unexpected that the liquid–vapor interface temperature will increase beyond the temperature of the impinging spray. The increase in interface temperature will be higher for higher partial pressures of air. As a result convective heat transfer coefficient based on difference between wall and interface temperature will increase with the wall temperature. However, the overall heat transfer coefficient based on the difference between wall and ambient temperature remains nearly constant (while accounting for the effect of variations in properties) until boiling begins.

3.1.1. Boiling regime

From Fig. 2 (system pressure of 101 kPa), with onset of boiling, the increase in the slope of the heat flux vs. T_w curve is observed for different flow rates, and different air partial pressures. It is noted that when $\frac{p_{air}}{p_{total}}$ is about 98%, the heat flux starts to vary non-linearly at a surface temperature of about 104 °C, whereas when $\frac{p_{air}}{p_{total}}$ is 3% heat flux starts to vary non-linearly at higher surface temperatures of about 120 °C. This indicates that evaporation at the liquid–vapor/gas interface tends to suppress nucleate boiling.

For all of the boiling heat flux data plotted against $T_w - T_{sat}$ (according to total pressure) in Fig. 6, it is found that at low wall superheats, lower spray temperatures give higher heat flux. This is due to the increased liquid subcooling for lower spray temperatures. All the data tend to merge at high surface temperatures. It is indicative of possible existence of fully developed nucleate boiling for the last few data points. In fully developed nucleate boiling heat flux is no longer dependent on partial pressure of air in the system as well as the spray temperature.

The dependence of heat flux on wall superheat is evaluated through $q \sim \Delta T_w^n$. The exponent of the $\Delta T_w = T_w - T_{sat}$ is found to be above 1, however the value is never more than 1.3, which means that forced convection is still playing a significant role after boiling starts and most of the data points are in partial nucleate boiling.

3.2. Heat transfer data obtained at different system pressures

The minimum vacuum level that could be reached was about 3.1 kPa (air partial pressure) using the closed system setup. Maintaining the same air pressure level,

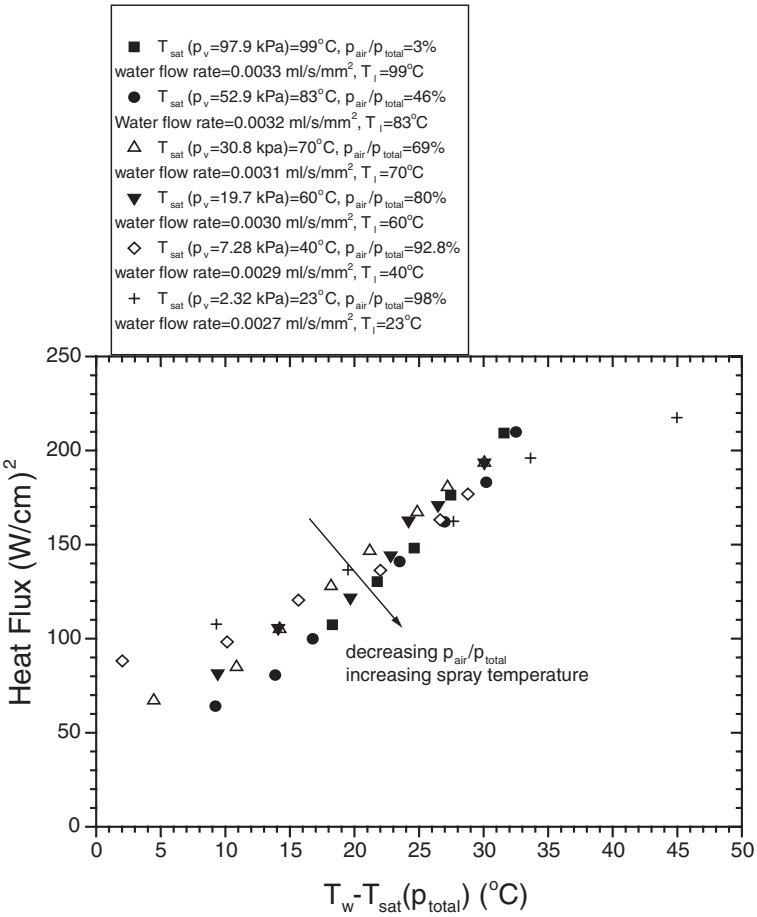

Fig. 6. Heat flux vs. surface superheat for different $\frac{p_{air}}{p_{total}}$ at 101 kPa system pressure after boiling starts.

while varying the vapor partial pressure from 7.3 kPa to 97.9 kPa, the total system pressure was varied from 10.4 kPa to 101 kPa, while the ratio of partial pressure of air, $\frac{p_{air}}{p_{total}}$, in the chamber varied from 3% to 29.8%. The saturation temperature corresponding to vapor pressure inside the chamber thus varied from about 100 °C to 40 °C. The temperature of the sprayed water in a given experiment was equal to the saturation temperature corresponding to the vapor pressure in the chamber.

Heat flux vs. T_w data at different system pressures and different partial pressures of air are shown in Fig. 7. It can be seen from the graph that in the single phase regime, the behavior is similar to the results discussed earlier in Section 3.1. At a certain surface temperature, the heat flux curves start to deviate from the linear variation as partial nucleate boiling begins. However only few data points deviate from the linear regime for each curve, and as a result, the difference between single phase and boiling is not discerned until the liquid film almost dries out. A dotted line is drawn on the graph, which separates the observed single phase regime and the possible partial nucleate boiling regime.

Single phase and boiling regimes are discussed separately in the following sections:

3.2.1. Single phase regime

Single phase overall heat transfer coefficient, is obtained as described earlier by dividing the heat flux with the difference between surface temperature and the vapor saturation temperature in the chamber,

$$h = \frac{q}{T_w - T_{sat}(P_v)}.$$

Nusselt number, Reynolds number and Prandtl number are evaluated at mean temperature between heater surface and spray. For a particular flow rate the data for different system pressures were found to fall on a single curve as was obtained when the system pressure was kept constant at 101 kPa, 72.5 kPa and 56 kPa (Fig. 4). It is found that in the single phase regime, heat transfer coefficient is not affected by the system pressure but

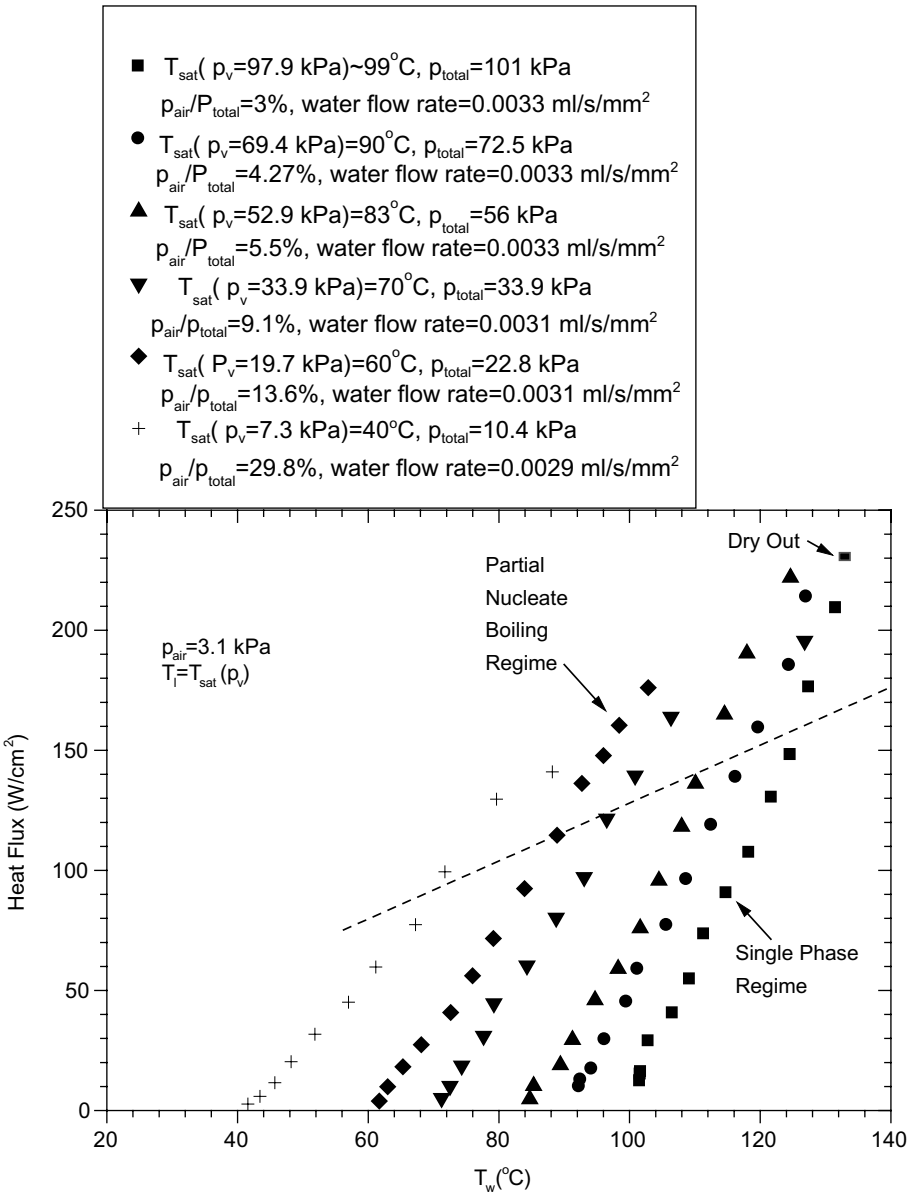

Fig. 7. Closed system spray cooling at different system pressures for flow rate of 0.0029 ml/s/mm^2.

depends on the partial pressure of air, $\frac{p_{air}}{p_{total}}$, in the chamber, as well as the flow rate. The ratio $\frac{Nu}{Nu_0}$ as a function of $\frac{p_{air}}{p_{total}}$ can be correlated as,

$$\frac{Nu}{Nu_0} = \left(\frac{p_{air}}{p_{total}}\right)^{-n} \tag{12}$$

where n depends on the flow rate. As can be noted from Fig. 4, n increases as flow rate decreases. For a flow rate of 0.0029 ml/s/mm^2 n is calculated to be 0.79 and for a flow rate of 0.0045 ml/s/mm^2 n is calculated to be 0.61.

3.2.2. Boiling regime

In the boiling regime, however, as the system pressure decreases, the corresponding system saturation temperature also decreases and boiling begins to occur at lower surface temperature. Heat flux vs. $T_w - T_{sat}(p_{total})$ is plotted in Fig. 8. It can be seen from Fig. 8 that in boiling regime the data set for different system pressures lie on distinct curves. It can also be seen from the graph that for the same superheat, higher system pressure yields higher heat flux.

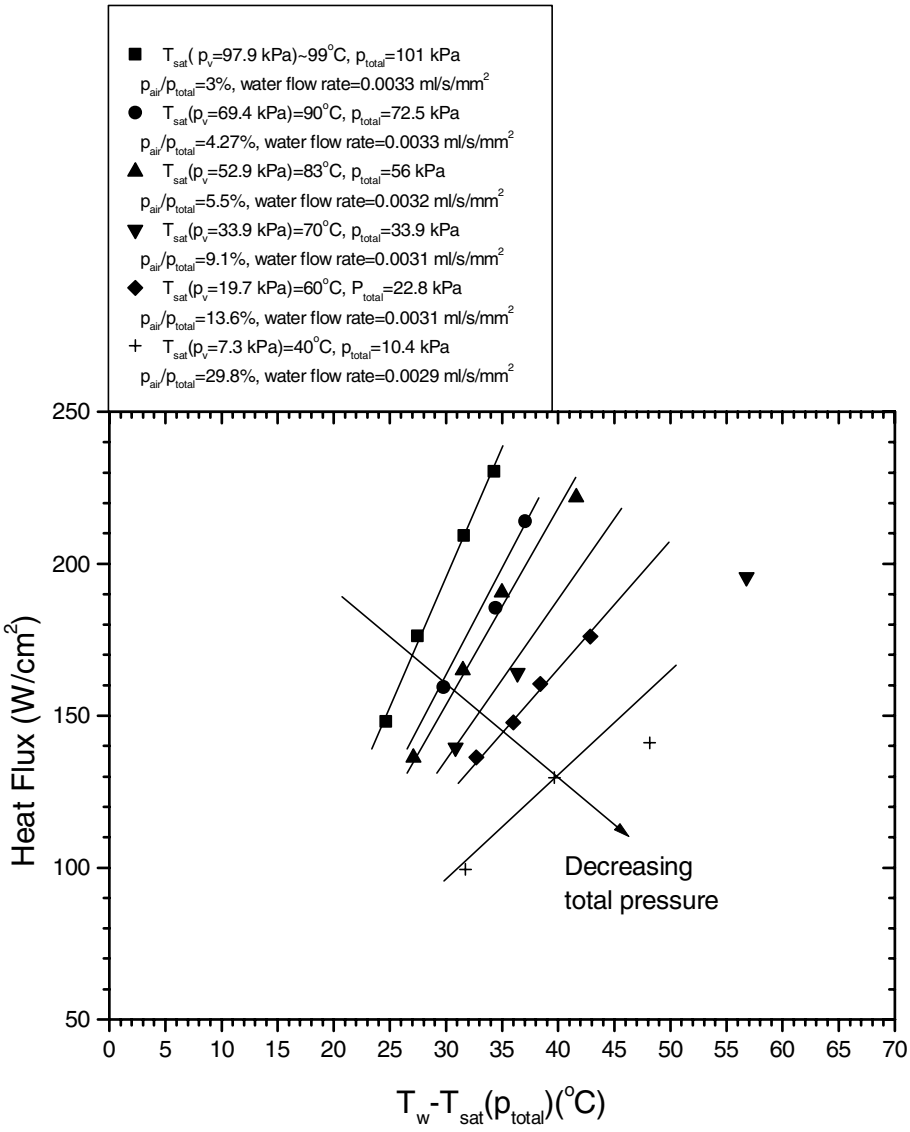

Fig. 8. Heat flux vs. surface superheat for different system pressures in the boiling regime.

In Fig. 8 the last point represents dry out at each system pressures. The dry out for low system pressures occur at lower surface temperatures. Dry out heat flux for each flow rate and at different system pressures is listed in Table 1. It is found from Fig. 8, when the system pressure is 10.4 kPa, dry out occurs at 141 W/cm^2, whereas, at higher system pressure of 101 kPa, dry out occurs at a heat flux greater than 230 W/cm^2. The last point for a pressure of 33.9 kPa is post dryout point. This suggests that dry out is not limited by liquid supply but is probably limited by the liquid that actually remains on the surface.

Before the surface dries out, there is mostly forced convection and little boiling occurring in the liquid film. Possible mechanisms for dry out are:

1. Liquid film becomes unstable at high evaporation rates.
2. Film breaks up because of the growth of bubbles at nucleation sites.

Dry out heat flux at different system pressures as obtained from the correlation of Mudawar et al. (Eq. (5)) with average orifice size, d_{orifice}, of 0.356 mm are compared in Table 1 with data from present experiments.

It can be seen that the prediction from Eq. (5) match the data from present experiments at high system pressures (101 kPa). However, when system pressure is low (10.4 kPa), the correlation of Mudawar et al. under-predicts CHF by about 45%. This may be because the vapor

Table 1
Dry out heat fluxes for different air percentage under the same system pressure of 101 kPa

	$\dot{V}_1$ (ml/s/mm^2)	Measured CHF (W/cm^2)	Predicted CHF (Eq. (5)) (W/cm^2)	Predicted CHF (Eq. (13)) (W/cm^2)
T_{sat} (p_v = 97.9 kPa) ~ 99 °C, p_{air} = 3.1 kPa,	0.0051	>230	318	371
p_{total} = 101 kPa, p_{air}/p_{total} = 3%	0.0033	>230	280	287
T_{sat} (p_v = 69.4 kPa) = 90 °C, p_{air} = 3.1 kPa,	0.0050	>226	263	323
p_{total} = 72.5 kPa, p_{air}/p_{total} = 4.27%	0.0033	224	231	250
T_{sat} (p_v = 52.9 kPa) = 83 °C, p_{air} = 3.1 kPa,	0.0050	225	222	287
p_{total} = 56 kPa, p_{air}/p_{total} = 5.5%	0.0032	221	195	222
T_{sat} (p_v = 30.8 kPa) = 70 °C, p_{air} = 3.1 kPa,	0.0049	196	134	201
p_{total} = 33.9 kPa, p_{air}/p_{total} = 9.1%	0.0031	184	117	155
T_{sat} (p_v = 19.7 kPa) = 60 °C, p_{air} = 3.1 kPa,	0.0031	176	103	143
p_{total} = 22.8 kPa, p_{air}/p_{total} = 13.6%				
T_{sat} (p_v = 7.3 kPa) = 40 °C, p_{air} = 3.1 kPa,	0.0029	141	78	125
p_{total} = 10.4 kPa, p_{air}/p_{total} = 29.8%				

density, ρ_v, dependence is not properly taken into account in their correlation. Based on the current experimental data, Eq. (5) is modified as,

$$\frac{q_{CHF}}{\rho_v h_{fg} \dot{V}} = 2.3 \left(\frac{\sigma}{\rho_l \dot{V}^2 d_{orifice}} \right)^{0.2} \left(\frac{\rho_l}{\rho_v} \right)^{0.5} \times \left(1 + 0.0019 \frac{\rho_l c_{p,l} \Delta T_{sub}}{\rho_v h_{fg}} \right) \quad (13)$$

The calculated values of CHF based on Eq. (13) are listed in Table 1. The predictions of CHF from Eq. (13) are within ±23%.

3.3. Effect of different parameters on heat removal with HAGO nozzle spray

The options for choosing the optimum parameters when using HAGO nozzle to cool an electronic component depends on several variables:

1) Flow rate:

As discussed earlier, in the single phase regime, higher liquid flow rate gives higher heat transfer coefficients. In the partial nucleate boiling regime, higher flow rate also yields higher heat fluxes because convection is still playing an important role. In fully developed nucleate boiling regime, all the curves for different flow rates merge together. The higher flow rate gives a higher dry out heat flux.

2) System pressure:

In the range of parameters studied, system pressure does not affect the heat transfer coefficient in single phase regime. After boiling starts, higher system pressure leads to higher heat flux for the same wall superheat, $T_w - T_{sat}(p_{total})$. Higher system pressure also yields higher dry out heat flux.

3) Partial pressures of air, $\frac{p_{air}}{p_{total}}$:

In the single phase regime, smaller values of $\frac{p_{air}}{p_{total}}$ give higher heat transfer coefficient because of the higher rate of evaporation at the liquid–gas interface. After fully developed boiling begins, heat flux no longer depends on $\frac{p_{air}}{p_{total}}$.

4) Liquid temperature:

Keeping the system pressure at 101 kPa, and the same ratio of partial pressure of air in the chamber, $\frac{p_{air}}{p_{total}} \sim 98\%$, the data were taken for 23 °C and 70 °C spray temperature. In single phase regime, slope of the heat transfer curve for 70 °C spray temperature is higher than that for 23 °C spray temperature. As the flow rate and spray environment are almost the same for the two cases, the increase in heat transfer coefficient is attributed to the difference in fluid properties. For the same flow rate, higher spray temperature (70 °C) gives a Reynolds number that is 2.6 times higher than that of 23 °C spray temperature. However Prandtl number for 70 °C water is about 2.6 times lower. Since Nusselt number strongly depends on Reynolds number (Eq. (11)), the observed 1.4 times increase in heat transfer coefficient is consistent with that predicted for Eq. (11).

After boiling begins the two sets of data start to merge together. In partial nucleate boiling regime, at a fixed $T_w - T_{sat}$, lower spray temperature gives higher heat flux because of the effect of liquid subcooling.

5) Pumping power:

Power needed for pumping the liquid through the HAGO nozzle is calculated as,

$$Q_{pumping} = \dot{V} A \Delta p \quad (14)$$

where $\dot{V}$ (ml/s/mm^2) is the volume flow rate through the HAGO nozzle and Δp (Pa) is the pressure drop across the HAGO nozzle. This pumping power does not

include losses in piping and fittings which can be substantial depending on how the system is configured. In this case, they were small. Total power removed from the heater surface is obtained as,

$$Q_{\text{removed}} = qA \tag{15}$$

where q is the measured heat flux from the heater surface, and A is the heater area. Ratio of pumping power to the total power removed, $Q_{\text{pumping}}/Q_{\text{removed}}$, is an indicator of the parasitic power used in achieving the required cooling rate.

Fig. 9 shows the calculated $Q_{\text{pumping}}/Q_{\text{removed}}$ as a function of surface temperature for different ratios of partial pressures of air, $\frac{p_{\text{air}}}{p_{\text{total}}}$, in the closed system when the system pressure was held constant at 101 kPa (Fig. 2).

It can be seen in Fig. 9 that $Q_{\text{pumping}}/Q_{\text{removed}}$ decreases non-linearly as surface temperature increases. In single phase regime, for the same system pressure, lower spray temperature gives the lowest ratio of pumping power to total power removed. Lower spray temperature gives higher heat flux whereas the pumping power is almost the same for a fixed flow rate. In fully developed boiling regime, the data for ratio of pumping power over total power removed merge together for all the cases tested while the total pressure is kept fixed at 101 kPa.

The calculated $Q_{\text{pumping}}/Q_{\text{removed}}$ as a function of surface temperature for all the cases in which p_{air} was fixed but total pressure was varied is shown in Fig. 10. Again, the ratio, $Q_{\text{pumping}}/Q_{\text{removed}}$ decreases non-linearly as surface temperature increases. In fully developed boiling regime, the pumping power to total power ratio for the same flow rate will overlap if data were plotted against $T_{\text{w}} - T_{\text{sat}}$ instead of T_{w}. It should be noted that the smallest value of the ratio of pumping power to heat removed decreases with increases in system pressure.

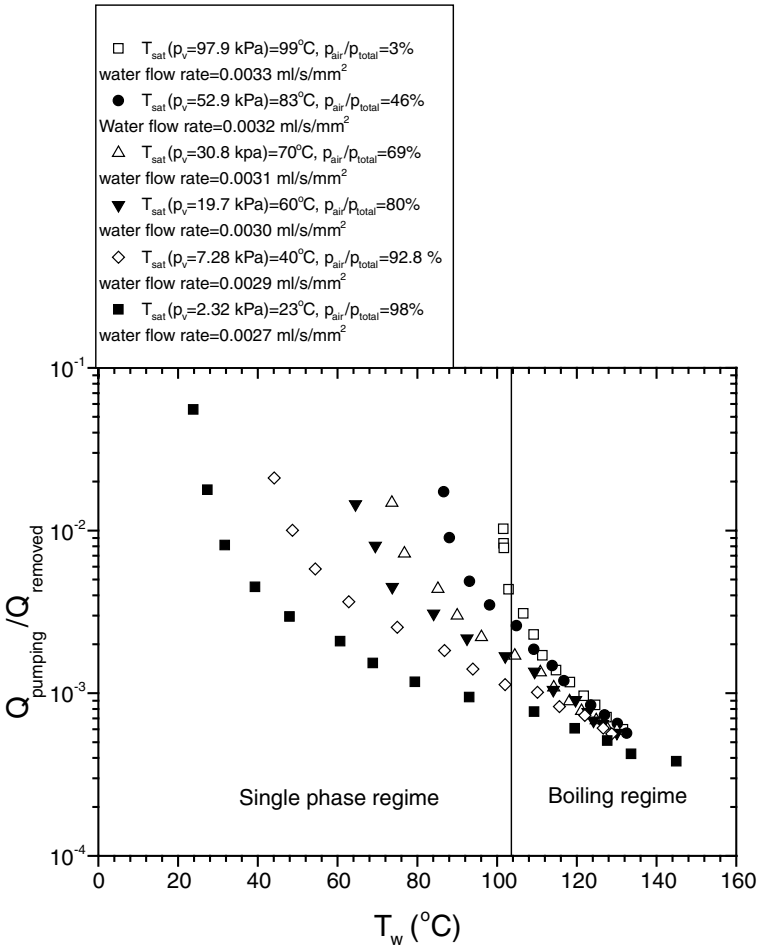

Fig. 9. Pumping power over total power removed vs. surface temperature for flow rate about 0.0029 ml/s/mm^2 at system pressure of 101 kPa.

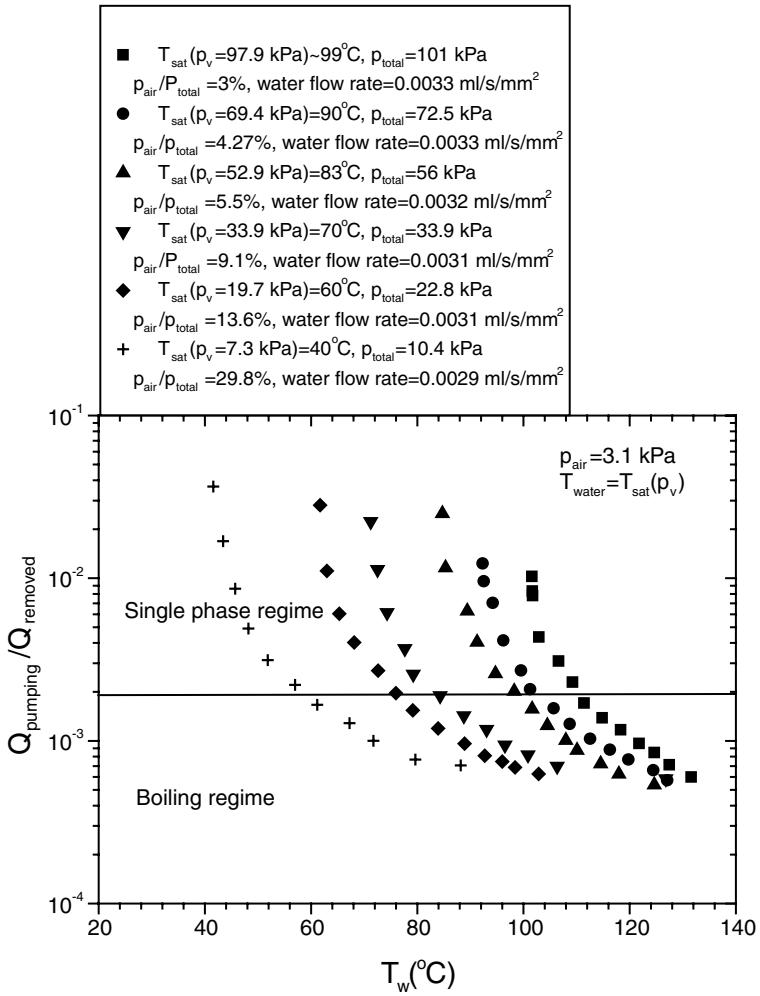

Fig. 10. Pumping power over total power removed vs. surface temperature under different system pressures at flow rate ~0.0029 ml/s/mm^2.

However, this reduction is accompanied by an increase in surface temperature.

4. Summary

Experiments with spray cooling were performed in both closed and open systems. In the single phase regime, from the measured wall temperature, heat fluxes, and liquid flow rate, a correlation for Nusselt number in single phase regime has been developed. Based on the correlation, Nusselt number varies as a function of $Re^{0.7}$ and $Pr^{1/3}$. Nusselt number is normalized with data in which evaporation is believed to be nearly zero. Normalized Nusselt number, $\frac{Nu}{Nu_0}$, decreases as ratio of partial pressure of air to total system pressure, $\frac{p_{air}}{p_{total}}$, increases. At a mass flux of 0.0029 ml/s/mm^2, normalized Nusselt number for $\frac{p_{air}}{p_{total}} \sim 3\%$ is four times higher than that for $\frac{p_{air}}{p_{total}} \sim 98\%$. This is caused by the higher evaporation rate in a system with less non-condensibles.

In the boiling regime, the heat flux is found to be unaffected by the partial pressure of non-condensibles in the system, but it depends on the total system pressure. Experimentally measured dry out heat fluxes at different system pressure were compared with those predicted from Mudawar et al.'s correlation. The correlation underestimates the dryout at low system pressures. A modified correlation based on the results of this study has been developed.

Acknowledgment

This work received support from DARPA.

References

[1] K.J. Choi, S.C. Yao, Mechanisms of film boiling heat transfer of normally impacting spray, Int. J. Heat Mass Transfer 30 (2) (1987) 311–318.
[2] S.C. Yao, K.J. Choi, Heat transfer experiments of monodispersed vertically impacting sprays, Multiphase Flow 5 (5) (1987) 639–648.
[3] A. Kopchikov, G.I. Veronin, T.A. Kolach, D.A. Labuntsov, P.D. Lebedev, Liquid boiling in a thin film, Int. J. Heat Mass Transfer 12 (1969) 791–896.
[4] M.R. Pais, L.C. Chow, E.T. Mahefkey, Surface roughness and its effects on the heat transfer mechanism in spray cooling, J. Heat Transfer 114 (1992) 211–219.
[5] M.S. Sehmbey, M.R. Pais, L.C. Chow, Effect of surface material properties and surface characteristics in evaporative spray cooling, J. Thermophys. Heat Transfer 6 (1992) 505–512.
[6] C. Bonacina, S. Del Giudice, G. Comini, Dropwise evaporation, J. Heat Transfer 101 (1979) 441–446.
[7] W.M. Grissom, F.A. Wierum, Liquid spray cooling of a heated surface, Int. J. Heat Mass Transfer 24 (1981) 261–271.
[8] K.A. Estes, I. Mudawar, Correlating of Sauter mean diameter and critical heat flux for spray cooling of small surface, Int. J. Heat Mass Transfer 38 (1995) 2985–2996.
[9] I. Mudawar, K.A. Estes, Optimizing and predicting CHF in spray cooling of a square surface, J. Heat Transfer 118 (1996) 672–680.
[10] S. Jiang, Heat removal using microjet arrays and microdroplets in open and closed systems for electronic cooling, PhD thesis, University of California, Los Angeles, CA, 2002.